

# Observational estimation of radiative feedback to surface air temperature over Northern High Latitudes

Jiwon Hwang<sup>1</sup> · Yong-Sang Choi<sup>1,2</sup>  · WonMoo Kim<sup>3</sup> · Hui Su<sup>2</sup> · Jonathan H. Jiang<sup>2</sup>

Received: 23 December 2016 / Accepted: 11 March 2017  
© Springer-Verlag Berlin Heidelberg 2017

**Abstract** The high-latitude climate system contains complicated, but largely veiled physical feedback processes. Climate predictions remain uncertain, especially for the Northern High Latitudes (NHL; north of 60°N), and observational constraint on climate modeling is vital. This study estimates local radiative feedbacks for NHL based on the CERES/Terra satellite observations during March 2000–November 2014. The local shortwave (SW) and longwave (LW) radiative feedback parameters are calculated from linear regression of radiative fluxes at the top of the atmosphere on surface air temperatures. These parameters are estimated by the de-seasonalization and 12-month moving average of the radiative fluxes over NHL. The estimated magnitudes of the SW and the LW radiative feedbacks in NHL are  $1.88 \pm 0.73$  and  $2.38 \pm 0.59 \text{ W m}^{-2} \text{ K}^{-1}$ , respectively. The parameters are further decomposed into individual feedback components associated with surface albedo, water vapor, lapse rate, and clouds, as a product of the change in climate variables from ERA-Interim reanalysis estimates and their pre-calculated radiative kernels. The results reveal the significant role of clouds in reducing the surface albedo feedback ( $1.13 \pm 0.44 \text{ W m}^{-2} \text{ K}^{-1}$  in the cloud-free condition, and  $0.49 \pm 0.30 \text{ W m}^{-2} \text{ K}^{-1}$  in the all-sky condition), while the lapse rate feedback is

predominant in LW radiation ( $1.33 \pm 0.18 \text{ W m}^{-2} \text{ K}^{-1}$ ). However, a large portion of the local SW and LW radiative feedbacks were not simply explained by the sum of these individual feedbacks.

**Keywords** Local radiative feedback · High-latitude climate feedback · Radiative kernel · Observational estimates of feedback

## 1 Introduction

Rapid warming over the Northern High Latitudes (NHL; poleward of 60°N) has occurred during the last few decades in both observations and climate model simulations (Hansen et al. 2005; Meehl et al. 2014). The ground observations show that the surface temperature over NHL increased at a rate of about 2–3 times faster than the global mean during the 1970–2008 period (Chylek et al. 2009). In the future, the increase of the NHL surface temperature is expected to be 1.5–4.5 times higher than that of the rest of the world (Holland and Bitz 2003; Comiso and Hall 2014; van der Linden et al. 2014). However, due to the complexity of the mechanisms behind the rapid warming in NHL, modeled climate characteristics are yet to be quantitatively intercompared among various climate models in high-latitude regions (Rind 2008). Up to date, the largest inter-model spread of the temperature response to CO<sub>2</sub> increment simulation is found over the Arctic (e.g., van der Linden et al. 2014). On the other hand, this large inter-model spread implies that climate models still misrepresent many underlying physical climate feedback processes (associated with snow/ice, cloud, and temperature profiles in NHL), as well as intrinsic nonlinearity among the feedback processes.

✉ Yong-Sang Choi  
ysc@ewha.ac.kr

<sup>1</sup> Department of Atmospheric Science and Engineering, Ewha Womans University, Engineer B 353, 52, Ewhayeodae-gil, Seodaemun-gu, Seoul 03760, Republic of Korea

<sup>2</sup> Jet Propulsion Laboratory, California Institute of Technology, Pasadena, CA, USA

<sup>3</sup> Climate Prediction Department, APEC Climate Center, Busan, Republic of Korea

Previous studies have demonstrated that the rapid local warming over NHL involves a number of radiative and dynamic feedback processes. They include surface albedo feedback (Hall 2004; Serreze et al. 2009; Screen and Simmonds 2010), atmospheric and oceanic transport feedback (e.g., Alexeev et al. 2005; Langen and Alexeev 2007; Graversen et al. 2008; Spielhagen et al. 2011), and cloud feedback (e.g., Vavrus 2004; Eastman and Warren 2010; Sedlar et al. 2011; Cesana et al. 2012; Kay and L'Ecuyer 2013; Cronin and Tziperman 2015). The conventional understanding is that reduced sea ice as a result of surface warming increases absorbed shortwave (SW) solar radiation at the surface, which accelerates Arctic warming. This process is active during the summer season (ice-albedo feedback). However, a recent study indicated that ice-albedo feedback associated with downwelling longwave radiation is also activated during the winter season (Burt et al. 2016). In response to the reduced sea ice and surface albedo, the increased temperature difference between near-surface and upper troposphere leads to less efficient outgoing longwave (LW) terrestrial radiation (lapse rate feedback), which serves as a positive feedback over NHL (Hansen et al. 1984; Manabe and Wetherald 1975). Pithan and Mauritsen (2014) confirmed that this temperature feedback would most significantly contribute to the high climate sensitivity in NHL, in addition to the ice-albedo feedback.

Cloud or moisture also plays a potentially important role in climate feedbacks over NHL. Ghatak and Miller (2013) suggested that increasing downward LW radiation associated with increasing atmospheric water vapor accelerates Arctic warming during the winter (water vapor feedback). However, it remains unclear how the changing NHL cloud fraction and property alter the transfer of both SW and LW radiation (cloud feedback). Various observational studies have found considerable uncertainties in the cloud radiative effect over NHL (Eastman and Warren 2010; Cesana et al. 2012; Kay and L'Ecuyer 2013), as the net cloud feedback is dependent on surface albedo, geographical location, seasonal characteristics, and cloud microphysical properties (Sedlar et al. 2011).

As an equally important issue, Graversen et al. (2008) suggested that atmospheric energy transport can blur the role of albedo feedback in the high-latitude region; however, the dynamic impact has been debated in recent studies (Hwang et al. 2011; Skific and Francis 2013). Also, the climate feedback processes can be nonlinearly coupled with each other and with other biogeochemical effects (Winton 2008; Chapin et al. 2008). Accordingly, the mere sum of known individual feedback processes is not necessarily identical to the total radiative feedback that determines the local climate sensitivity in NHL. To clarify these issues, the total of individual feedbacks constituting the NHL

climate system should, above all, be estimated based on the observed broadband (visible to infrared) radiation data.

The aim of this study is to quantitatively estimate the magnitude of local radiative feedbacks in the NHL, and thus understand the climate changes in the NHL. To this end, this study uses monthly broadband radiation data from the Clouds and the Earth's Radiant Energy System (CERES) on *Terra* satellite, whose data have been collected over the entire NHL since 2000 (Wielicki et al. 1996). We further discriminate the relative contributions of atmospheric temperatures, surface albedo, water vapor, and non-linear residuals to the local radiative feedback process over the NHL.

## 2 Data and method

### 2.1 Data description and removal of seasonality

The monthly  $2.5^{\circ}$ -gridded TOA outgoing SW radiation ( $R_{SW}^{\uparrow}$ ), outgoing LW radiation ( $R_{LW}^{\uparrow}$ ), and surface albedo ( $\alpha$ ) were obtained from the CERES data (the ES4 Terra-Xtrk Edition 3 product at [http://eosweb.larc.nasa.gov/project/ceres/ceres\\_table](http://eosweb.larc.nasa.gov/project/ceres/ceres_table)) (Wielicki et al. 1996). All the variables are available for all-sky and clear-sky conditions. The uncertainty of the SW and LW radiations at TOA directly measured by the CERES is  $\sim 5$  and  $\sim 1\%$ , respectively (CERES Science Team 2013).

To examine the contribution of climate variables to local radiative feedbacks, we also obtained monthly  $1.5^{\circ}$ -gridded atmospheric variables, including the surface air temperatures at 2-m height ( $T_s$ ), vertical profiles of temperature ( $T$ ), and specific humidity ( $q$ ) from the ERA-Interim reanalysis dataset. This dataset was produced by the European Centre for Medium-Range Weather Forecasts (ECMWF) (available at <http://apps.ecmwf.int/datasets/>) (Dee et al. 2011).

The aforementioned variables were taken within NHL from the period of March 2000 to November 2014. The data were de-seasonalized by subtracting the climatology of 2000–2014 monthly means at each grid point, and then area-averaged over the NHL ( $\langle x \rangle$ , where  $x$  is an anomaly). Otherwise, strong seasonality and non-feedback cloud variations in the time series would mask the feedback signals (Choi et al. 2014a). For example, surface temperature and absorbed SW radiation in summer are larger than those in winter. This seasonality creates a high correlation between the two variables, which does not necessarily imply the presence of strong SW feedback between the two variables.

Even though all the anomalies are de-seasonalized, they still contain higher-order seasonal variation. Figure 1 shows the de-seasonalized and area-averaged monthly anomalies,  $\langle R_{SW}^{\uparrow} \rangle$ ,  $\langle R_{LW}^{\uparrow} \rangle$ , and  $\langle T_s \rangle$ , for each year from 2000 to 2014.

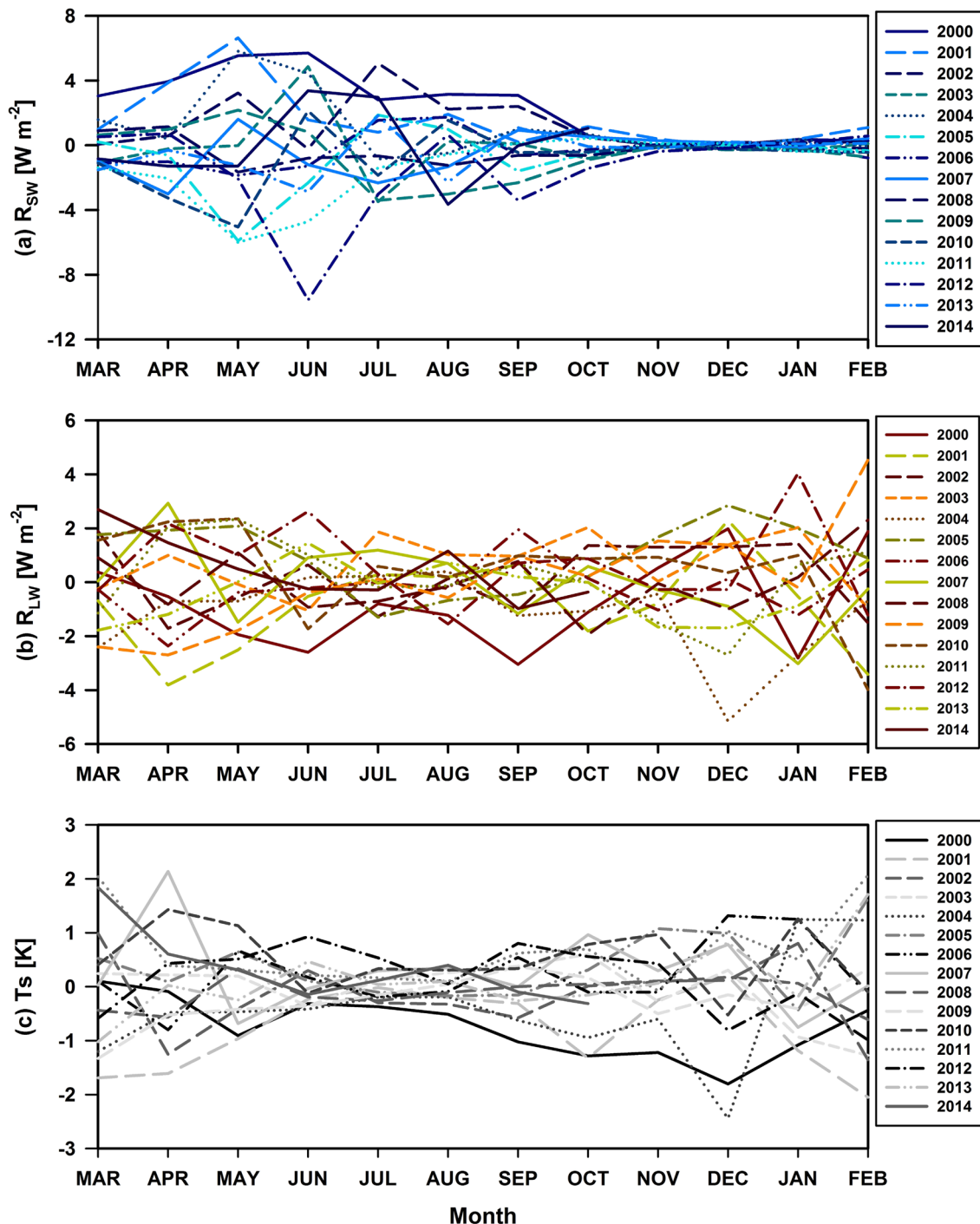


**Fig. 1** Deseasonalized area-averaged monthly anomalies of **a** outgoing shortwave radiation, **b** outgoing longwave radiation, and **c** surface air temperature, for each year from 2000 to 2014

$\langle R_{SW}^{\uparrow} \rangle$  is highly variable from March to September, while it remains near zero during winter months (December–February) (Fig. 1a). On the other hand, the seasonal variations are not apparent in  $\langle R_{LW}^{\uparrow} \rangle$  (Fig. 1b).  $\langle T_s \rangle$  shows little change during the months from June to August, which correspond

to the sea ice melting season (Fig. 1c). This implies that the solar radiation and sea ice retain the seasonality in the anomalies. Furthermore, the slow feedback processes that operate for several months (such as the ice-albedo feedback process) should be taken into account in our feedback estimation.

To exclude the remaining seasonality in the time series while retaining radiative feedback processes with time spans longer than a month (Choi and Song 2012), we took forward 12-month moving averages of  $\langle x \rangle$  ( $\langle \tilde{x} \rangle$ ). Fig. 2 shows that the seasonal dependency is much reduced in the 12-month moving averages of  $\langle R_{SW}^\uparrow \rangle$ ,  $\langle R_{LW}^\uparrow \rangle$ , and  $\langle T_s \rangle$  (hereafter denoted as  $\widetilde{\langle R_{SW}^\uparrow \rangle}$ ,  $\widetilde{\langle R_{LW}^\uparrow \rangle}$  and  $\widetilde{\langle T_s \rangle}$ ). We show later that if the 12-month moving averages are not taken, the estimated magnitude of local radiative feedback is unstable.

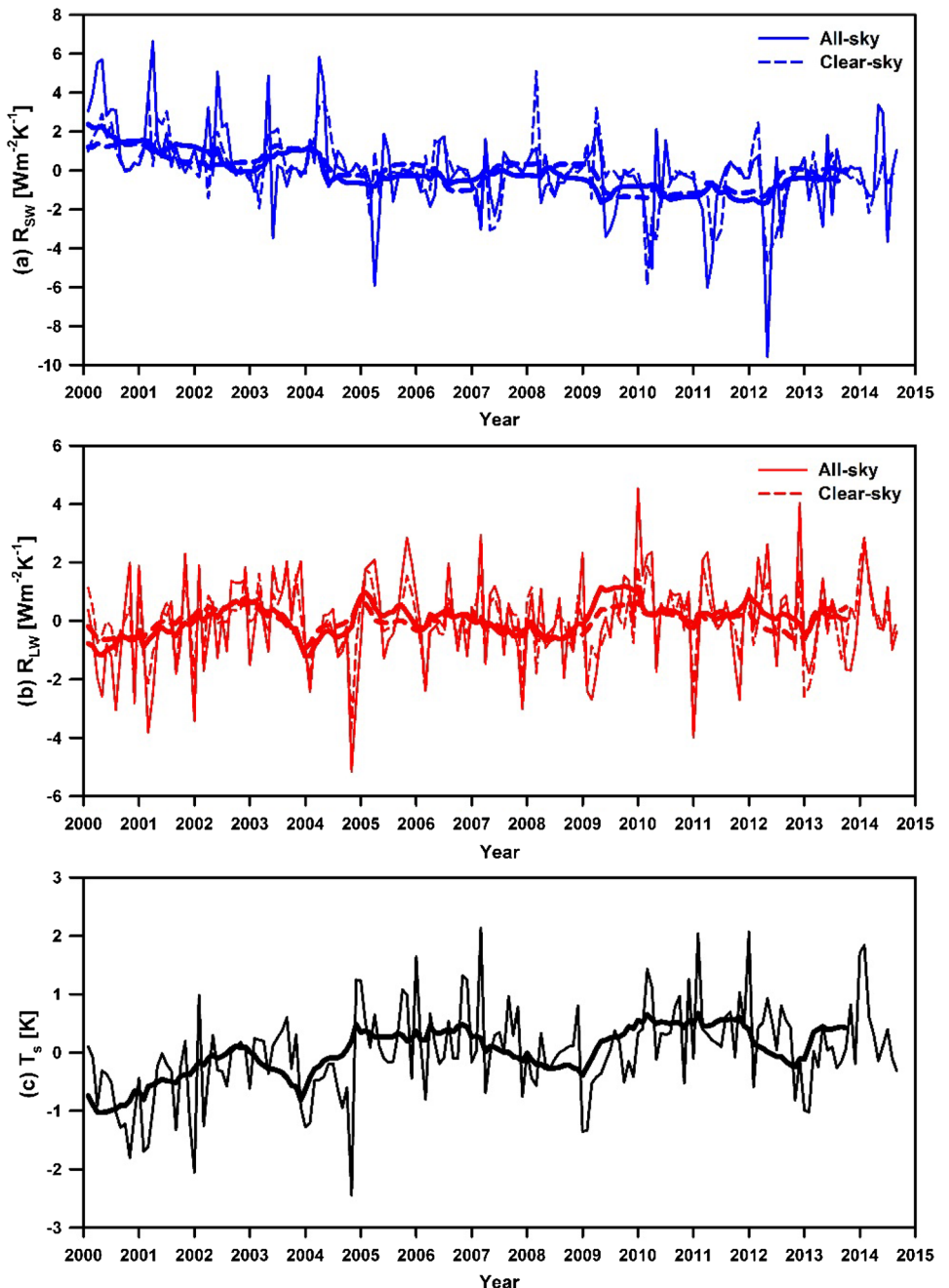
## 2.2 Total local radiative feedback estimation through a simple linear regression

We shall begin with the standard linearized local-scale domain energy balance:

$$-\left[ \langle R_{SW}^\uparrow \rangle + \langle R_{LW}^\uparrow \rangle \right] = F_{SW} + F_{LW} + (\lambda_{SW} + \lambda_{LW}^*) T_s + \int (\vec{D} \cdot \vec{n}) dl, \quad (1)$$

where the anomalies in the net TOA radiations are indicated by  $-\left[ \langle R_{SW}^\uparrow \rangle + \langle R_{LW}^\uparrow \rangle \right]$ ;  $F_{SW}$  and  $F_{LW}$  are the radiative

**Fig. 2** NHL average monthly and 12-months moving averaged anomalous time series for **a** outgoing shortwave radiation, **b** outgoing longwave radiation, and **c** surface air temperature for all-sky (solid line) and clear-sky (dashed line) conditions for March 2000 to November 2014, from CERES and ERA-Interim



forcing in SW and LW radiation, respectively;  $\lambda_{SW}\langle T_s \rangle$  and  $\lambda_{LW}^*\langle T_s \rangle$  are the SW and LW radiative responses to the changes in surface temperature, respectively (the asterisk in  $\lambda_{LW}^*\langle T_s \rangle$  indicates the inclusion of the Planck response); and the integral summarizes the dynamical heat transport perturbation from atmosphere or ocean into the local domain ( $\vec{D}$  is a dynamical heat flux;  $\vec{n}$  is a unit vector normal to the boundary of the domain, direct inward; and  $dl$  is an element of length along the boundary) (Gregory et al. 2004; Forster and Gregory 2006; Donohoe et al. 2014; Trenberth et al. 2015). The positively valued  $\lambda$  is defined as the local radiative feedback parameter for NHL, i.e., the TOA downwelling radiative response for a positive temperature perturbation in units of  $\text{W m}^{-2} \text{K}^{-1}$  (Knutti and Hegerl 2008; Christensen et al. 2016).

The estimation of the feedback parameter is normally based on the sea surface temperature (SST) change (Lindzen and Choi 2009, 2011). However, excluding the land and ice-covered ocean from NHL, the water-covered ocean takes a relatively small proportion in NHL. Moreover, the variation in the ice-covered ocean is the most typical geographic feature in NHL and the northern polar cap, and is driven by sensible and latent heat flux that strongly depends on the surface air temperature (SAT) change (Rigor et al. 2000). Hence, SAT over NHL was used for  $T_s$  in this study.

The local SW and LW radiative feedback parameters for NHL are estimated from the linear regressions of  $\widetilde{\langle R_{SW}^\uparrow \rangle}$  and  $\widetilde{\langle R_{LW}^\uparrow \rangle}$  on  $\widetilde{\langle T_s \rangle}$ , assuming that the long-term trend in radiative forcing in Eq. (1) can be ignored for the period considered here (Santer et al. 2014; Trenberth et al. 2015), and that the integral term in Eq. (1) remains approximately unchanged (Donohoe et al. 2014):

$$\lambda_{SW|NHL} \approx -\frac{\Delta \widetilde{\langle R_{SW}^\uparrow \rangle}}{\Delta \widetilde{\langle T_s \rangle}} \quad (2a)$$

and,

$$\lambda_{LW|NHL} \approx -\frac{\Delta \widetilde{\langle R_{LW}^\uparrow \rangle}}{\Delta \widetilde{\langle T_s \rangle}} - \lambda_p, \quad (2b)$$

where, the monthly perturbation is denoted as  $\Delta$ . Note that the estimated local LW radiative feedback parameter ( $\lambda_{LW|NHL}$ ) is defined as the linear regression coefficient minus the Planck response, which implies the response of TOA LW radiation being absorbed by the system to changes in surface air temperature. Here, the Planck response parameter ( $\lambda_p$ ) was roughly assumed to be  $-3.24 \pm 0.51 \text{ W m}^{-2} \text{K}^{-1}$  for the NHL, following the Planck response ( $-\lambda_p \Delta T_s^* = \Delta R_{LW}^\uparrow$ ) (Cess 1976): assuming the absence of other feedback processes and constant effective emissivity, the observed TOA outgoing LW radiations and

surface temperatures ( $T_s^*$ ) follows only the Stefan–Boltzmann law ( $R_{LW}^\uparrow = \sigma(T_s^*)^4$ ) (the asterisk in  $T_s^*$  signifies estimated surface temperature based on the Stefan–Boltzmann law, which is different from the observed  $T_s$ ). Hereafter, the symbol  $\lambda$  is a short-handed notation of  $\lambda|_{NHL}$ .

The lagged correlation and regression analyses effectively investigate the accurate local radiative feedback parameter. Assuming that the climate variation is mainly signified by surface temperature and radiation, the regression slope should represent the radiative feedback signal, with the maximum correlation at the zero time lag (Frankignoul et al. 1998; Frankignoul 1999; Spencer and Braswell 2011; Choi et al. 2014a). This study carried out the lagged correlation and regression analyses for  $\widetilde{\langle R_{SW}^\uparrow \rangle}$ ,  $\widetilde{\langle R_{LW}^\uparrow \rangle}$ , and  $\widetilde{\langle T_s \rangle}$ ; and obtained the total local SW and LW radiative feedback parameters from the zero-lag regression slope, as in Eq. (2a, 2b).

The ‘local’ term of the local radiative feedback parameters obtained in this study indicates only the radiative response to the change in the surface (air) temperature. Namely, it is not a quantity that can be directly converted to effective climate sensitivity. This is both because the NHL climate is not a closed system, and the present calculation does not fully involve the heat transport between NHL and the surroundings.

### 2.3 Individual feedback estimation through a radiative kernel method

The individual feedback parameters were quantitatively estimated from the radiative kernel method (Soden and Held 2006; Soden et al. 2008; Shell et al. 2008; Dessler 2013). The total local SW and LW radiative feedback parameters ( $\lambda_{SW}$  and  $\lambda_{LW}$ ) estimated from Eq. (2a, 2b) can be decomposed into individual feedback components:

$$\lambda_{SW} = \lambda_\alpha + \lambda_{c,SW} + \lambda_{Res,SW} \quad (3a)$$

and,

$$\lambda_{LW} = \lambda_L + \lambda_w + \lambda_{c,LW} + \lambda_{Res,LW}, \quad (3b)$$

where,  $\lambda_\alpha$ ,  $\lambda_L$ , and  $\lambda_w$  are the feedback parameters associated with albedo, lapse rate, and water vapor, respectively; and  $\lambda_{c,SW}$  and  $\lambda_{c,LW}$  are cloud feedback parameters for SW and LW, respectively. The residual feedback parameters ( $\lambda_{Res,SW}$  and  $\lambda_{Res,LW}$ ), which mainly originate from the atmospheric heat transport and the oceanic heat exchange, were calculated by subtracting the sum of individual feedback parameters from the total local radiative feedback parameter (Kim et al. 2015). Also, the nonlinearities among the internal feedback processes could partially affect the residual feedback parameter (Choi et al. 2014b). The shortwave water vapor feedback was not considered in this study, since the shortwave absorption by water vapor

is not primary. In either case, this would be included in the residual term.

In the radiative kernel method, each feedback parameter is composed of two parts. The first part is the radiative kernel ( $K_x$ ), driven from the response of TOA radiation to the climate variables ( $\alpha, T, q$ ) changes (i.e.,  $K_x = \partial R/\partial x$ ); and the second part is the response of the climate variables to the changing surface temperature. Each feedback component can be calculated from the following equations:

$$\lambda_\alpha = K_\alpha \frac{\Delta\langle\widetilde{\alpha}\rangle}{\Delta\langle\widetilde{T}_s\rangle} \quad (4)$$

$$\lambda_w = \sum K_w \frac{\Delta\langle\widetilde{q}\rangle}{\Delta\langle\widetilde{T}_s\rangle} \quad (5)$$

$$\lambda_L = \sum K_T \frac{\Delta(\langle\widetilde{T}\rangle - \langle\widetilde{T}_s\rangle)}{\Delta\langle\widetilde{T}_s\rangle} \quad (6)$$

where, the  $K_x$ 's [the albedo kernel ( $K_\alpha$ ), the water vapor kernel ( $K_w$ ), and the temperature kernel ( $K_T$ )], were obtained from the annual mean radiative feedback kernels for the Community Atmospheric Model version 3 (CAM3), from the National Center for Atmospheric Research (NCAR). Prior to the analysis, all of the kernels were averaged regionally and annually, because the  $K_x$ 's are functions of the latitude, longitude, and month of year. The total derivatives ( $\Delta\langle\widetilde{x}\rangle/\Delta\langle\widetilde{T}_s\rangle$ ) were estimated from the slope of the linear regression line between the time variations in climate variables and  $T_s$ . Except for the albedo feedback, the water vapor and lapse rate feedback parameters are functions of altitude. Thus they were vertically integrated from the surface to the tropopause (defined as 300 hPa for NHL), which is denoted as  $\Sigma$ .

The surface albedo and water vapor feedbacks were calculated from the product of the kernel and the regression slope of the changes in albedo and specific humidity, as in Eqs. (4) and (5); and the lapse rate feedback was calculated from the product of the kernel and the changes in temperature difference between the upper level and surface, as in Eq. (6). Table 1 lists the calculated values of  $\Delta\langle\widetilde{x}\rangle/\Delta\langle\widetilde{T}_s\rangle$ ,  $K_x$ , and  $\lambda_x$ .

The cloud feedback components for each SW ( $\lambda_{c,SW}$ ) and LW ( $\lambda_{c,LW}$ ) radiation were estimated from the differences between clear-sky ( $K_x^0$ ) and all-sky kernels ( $K_x$ ) (Soden et al. 2008; Jonko et al. 2012; Shell et al. 2008; Kim et al. 2015):

$$\lambda_{c,SW} = \frac{\Delta C_{RF,SW}}{\Delta\langle\widetilde{T}_s\rangle} + (K_\alpha - K_\alpha^0) \left( \frac{\Delta\langle\widetilde{\alpha}\rangle}{\Delta\langle\widetilde{T}_s\rangle} \right) \quad (7a)$$

$$\begin{aligned} \lambda_{c,LW} &= \frac{\Delta C_{RF,LW}}{\Delta\langle\widetilde{T}_s\rangle} + \sum (K_T^0 - K_T) \left( \frac{\Delta\langle\widetilde{T}\rangle}{\Delta\langle\widetilde{T}_s\rangle} \right) \\ &\quad + \sum (K_w^0 - K_w) \left( \frac{\Delta\langle\widetilde{q}\rangle}{\Delta\langle\widetilde{T}_s\rangle} \right) \end{aligned} \quad (7b)$$

The changes in cloud radiative forcing ( $\frac{\Delta C_{RF}}{\Delta\langle\widetilde{T}_s\rangle}$ ) for the

SW and LW were calculated from the difference between the total local radiative feedback parameter for the all-sky ( $\lambda_{SW}$  and  $\lambda_{LW}$ ) and the clear-sky conditions ( $\lambda_{SW}^0$  and  $\lambda_{LW}^0$ ), and the cloud radiative effect originating from each variable was calculated based on Eqs. (3a, 3b)–(6).

### 3 Results

#### 3.1 Total local shortwave and longwave radiative feedback parameters

The lag-month regression analysis based on Eq. (2a, 2b) provides the magnitudes of local radiative feedback parameters in NHL (Fig. 3). The thin lines come from the unsmoothed time series without the 12-month moving average ( $\langle x \rangle$ ), and the thick lines come from the smoothed time series with the 12-month moving average ( $\langle \widetilde{x} \rangle$ ). A negative lag means that the outgoing radiative perturbations are ahead of  $T_s$ , while a positive lag means that  $T_s$  is ahead of the outgoing radiative perturbations. The lagged correlations of  $\langle R_{SW}^\uparrow \rangle$  and  $\langle R_{LW}^\uparrow \rangle$  with  $\langle T_s \rangle$  are distorted, whereas those of  $\langle R_{SW}^\uparrow \rangle$  and  $\langle R_{LW}^\uparrow \rangle$  with  $\langle \widetilde{T}_s \rangle$  show a gentle convex curve with maximum/minimum correlations at the zero lag. In particular, the correlation of  $\langle R_{SW}^\uparrow \rangle$  and  $\langle T_s \rangle$  shows a noticeable discrepancy between the unsmoothed and smoothed cases. The distorted curves and the relatively low correlations (thin line in Fig. 3a) imply that its monthly time variations hardly reveal the radiative response over NHL. On the other hand, the zero-lag correlations for the smoothed case (thick line in Fig. 3a) are clearly distinguishable as 0.81 and 0.85 for SW (−0.68 and −0.65 for LW) for the all-sky and clear-sky conditions, respectively.

The regression slopes peak at the zero time lag, which is in line with the correlation patterns (Fig. 3b). The positive slope for SW radiation is driven by the increased downward radiation per surface air warming, indicating a positive feedback parameter. The magnitudes ± the standard errors of the absorbed SW radiation per 1 K rising in SAT are found to be  $+1.88 \pm 0.73$  and  $+1.65 \pm 0.55 \text{ W m}^{-2} \text{ K}^{-1}$ , in the all-sky and clear-sky conditions, respectively. This is a direct indication of the local SW radiative feedback. Likewise, the LW

**Table 1** Results of regression coefficients of changes in climate variables ( $\alpha, T, q$ ) to the surface temperature changes ( $\Delta\langle\widetilde{x}\rangle/\Delta\langle\widetilde{T}_s\rangle$ ), NHL average of radiative kernels ( $K_x$ ), and feedback values

Variable ( $x$ )	Altitude (hPa)	$\Delta\langle\widetilde{x}\rangle/\Delta\langle\widetilde{T}_s\rangle$	Kernel ( $K_x$ )	Feedback ( $\lambda_x$ )	Feedback value ( $\text{W m}^{-2} \text{K}^{-1}$ )	Vertically integrated feedback value ( $\text{W m}^{-2} \text{K}^{-1}$ )
Surface albedo ( $\alpha$ )	Surface	$-0.84 \pm 0.33$ ( $-0.84 \pm 0.29$ )	$-0.58$ ( $-1.34$ )	Surface albedo ( $\lambda_\alpha$ )	$+0.49 \pm 0.30$ ( $+1.13 \pm 0.44$ )	–
Temperature ( $T$ )	300	$-0.10 \pm 0.11$	$-0.28$ ( $-0.16$ )	Lapse rate ( $\lambda_L$ )	$+0.31 \pm 0.09$ ( $+0.18 \pm 0.03$ )	$1.33 \pm 0.18$ ( $0.92 \pm 0.08$ )
	400	$+0.25 \pm 0.11$	$-0.32$ ( $-0.21$ )		$+0.24 \pm 0.06$ ( $+0.16 \pm 0.03$ )	
	500	$+0.26 \pm 0.12$	$-0.28$ ( $-0.23$ )		$+0.21 \pm 0.04$ ( $+0.17 \pm 0.03$ )	
	600	$+0.23 \pm 0.13$	$-0.25$ ( $-0.21$ )		$+0.19 \pm 0.05$ ( $+0.16 \pm 0.03$ )	
	700	$+0.29 \pm 0.13$	$-0.28$ ( $-0.21$ )		$+0.20 \pm 0.06$ ( $+0.15 \pm 0.04$ )	
	850	$+0.55 \pm 0.17$	$-0.28$ ( $-0.18$ )		$+0.13 \pm 0.07$ ( $+0.08 \pm 0.04$ )	
	925	$+0.82 \pm 0.24$	$-0.33$ ( $-0.15$ )		$+0.06 \pm 0.09$ ( $+0.03 \pm 0.04$ )	
	1000	$+1.00 \pm 0.28$	$-0.09$ ( $-0.02$ )		$+0.00 \pm 0.00$ ( $+0.00 \pm 0.00$ )	
Specific humidity ( $q$ )	300	$+0.03 \pm 0.01$	$+0.15$ ( $+0.18$ )	Water vapor ( $\lambda_q$ )	$+0.00 \pm 0.00$ ( $+0.01 \pm 0.00$ )	$0.08 \pm 0.02$ ( $0.22 \pm 0.14$ )
	400	$+0.06 \pm 0.04$	$+0.16$ ( $+0.21$ )		$+0.01 \pm 0.01$ ( $+0.01 \pm 0.01$ )	
	500	$+0.10 \pm 0.07$	$+0.13$ ( $+0.19$ )		$+0.01 \pm 0.01$ ( $+0.02 \pm 0.01$ )	
	600	$+0.26 \pm 0.14$	$+0.09$ ( $+0.14$ )		$+0.02 \pm 0.01$ ( $+0.04 \pm 0.02$ )	
	700	$+0.68 \pm 0.25$	$+0.04$ ( $+0.09$ )		$+0.03 \pm 0.02$ ( $+0.06 \pm 0.04$ )	
	850	$+1.89 \pm 0.60$	$+0.00$ ( $+0.03$ )		$+0.00 \pm 0.00$ ( $+0.06 \pm 0.10$ )	
	925	$+2.47 \pm 0.77$	$-0.00$ ( $+0.01$ )		$-0.00 \pm 0.00$ ( $+0.02 \pm 0.10$ )	
	1000	$+2.40 \pm 0.72$	$-0.00$ ( $+0.00$ )		$-0.00 \pm 0.00$ ( $-0.00 \pm 0.00$ )	

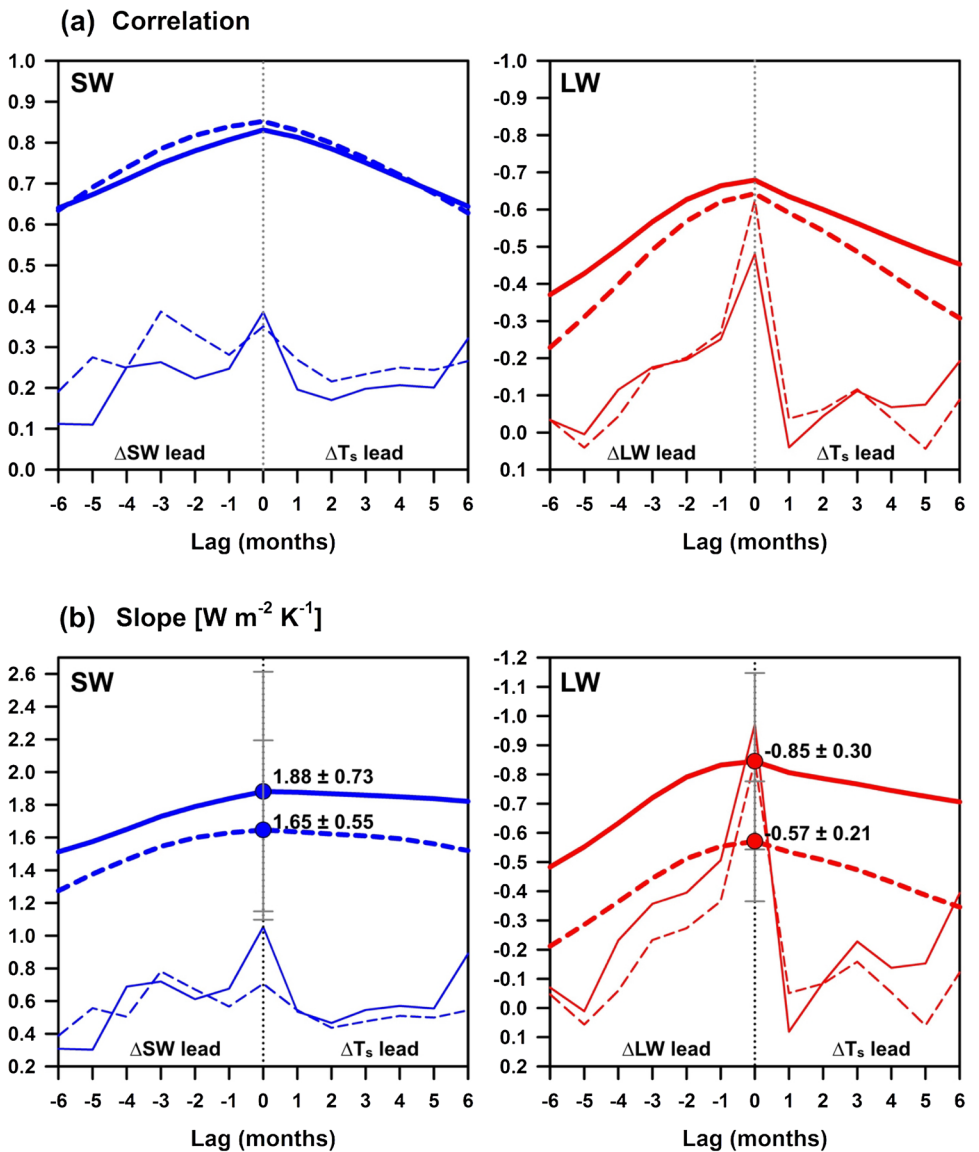
The corresponding values at the clear-sky condition are listed in parentheses

radiative response to 1 K rising in SAT is  $-0.85 \pm 0.30$  and  $-0.57 \pm 0.21 \text{ W m}^{-2} \text{ K}^{-1}$ , respectively. However, the negative slope for LW radiation does not necessarily imply a negative radiative response, because the Planck response essentially contributes to the large negative slope. Subtracting the Planck response ( $-3.24 \pm 0.51 \text{ W m}^{-2} \text{ K}^{-1}$ ) from these slopes, the local LW radiative feedback parameters can be estimated as  $+2.38 \pm 0.59$  and  $+2.66 \pm 0.55 \text{ W m}^{-2} \text{ K}^{-1}$  in the all-sky and clear-sky conditions, respectively. Consequently, the net local radiative feedback over NHL is approximated to be  $+4.26 \pm 1.32$  and  $+4.31 \pm 1.10 \text{ W m}^{-2} \text{ K}^{-1}$  in the all-sky and clear-sky conditions, respectively. However, if the unsmoothed time variations are applied to local

radiative feedback estimation (thin line in Fig. 3b), the local radiative feedback parameter could be under- or over-estimated, because the seasonality or randomly varying clouds can affect the monthly perturbations of the radiations and temperature.

The results provide an important implication in the general observationally based feedback estimation. In recent years, several attempts have been made to estimate the tropical and global climate feedback strengths from the lagged correlation analysis with satellite-observed TOA radiation and surface temperature (Gregory et al. 2004; Forster and Gregory 2006; Murphy 2010; Lindzen and Choi 2009, 2011; Trenberth et al. 2015). In principle, the largest covariance occurs at simultaneous time (or

**Fig. 3** a Lagged correlation, and b regression coefficient of outgoing shortwave (blue) and longwave (red) radiative perturbations on surface air temperature changes using anomalies in monthly time variations (filtered, thin lines) and 12-months moving averaged time variations (filtered, thick lines); the solid line indicates all sky condition, and the dashed line indicates clear sky condition. The error bars indicate standard error of the regression coefficients



month) under strong feedback processes between the two variables; moreover, the regression slope was necessarily identical to the feedback parameter according to several transient climate simulations of an energy balance model (Choi et al. 2014a). However, when confining the domain to a local domain like NHL, it has been very difficult to obtain the largest covariance at simultaneous time, since the lagged covariance becomes larger than the zero-lag covariance. This distortion was found to result from natural non-feedback factors, such as randomly varying clouds, horizontal heat/moisture transport, and strong seasonal changes (Choi et al. 2014a). Thus, it can be said that the present results in Fig. 3 avoided the disturbance of all these non-feedback factors, and revealed reliable local feedback signals from the observations.

### 3.2 Individual feedback parameters for climate variables

We now investigate the contributions of individual climate variables to the total radiative feedbacks. To understand the contribution of surface albedo to the local radiative feedback, Fig. 4 shows the latitude-longitude distributions of surface albedo response to the increased SAT, surface albedo kernel, and surface albedo feedback. Figure 4a presents the regression slope of  $\Delta\tilde{\alpha}$  versus  $\Delta\tilde{T}_s$  at each grid box. In the Arctic Ocean, the slope is mostly negative, and the surface albedo decreases with the SAT, probably due to sea ice retreat. The surface albedo kernel is annually averaged at each grid point, and the negative sign means that the increase in surface albedo derives

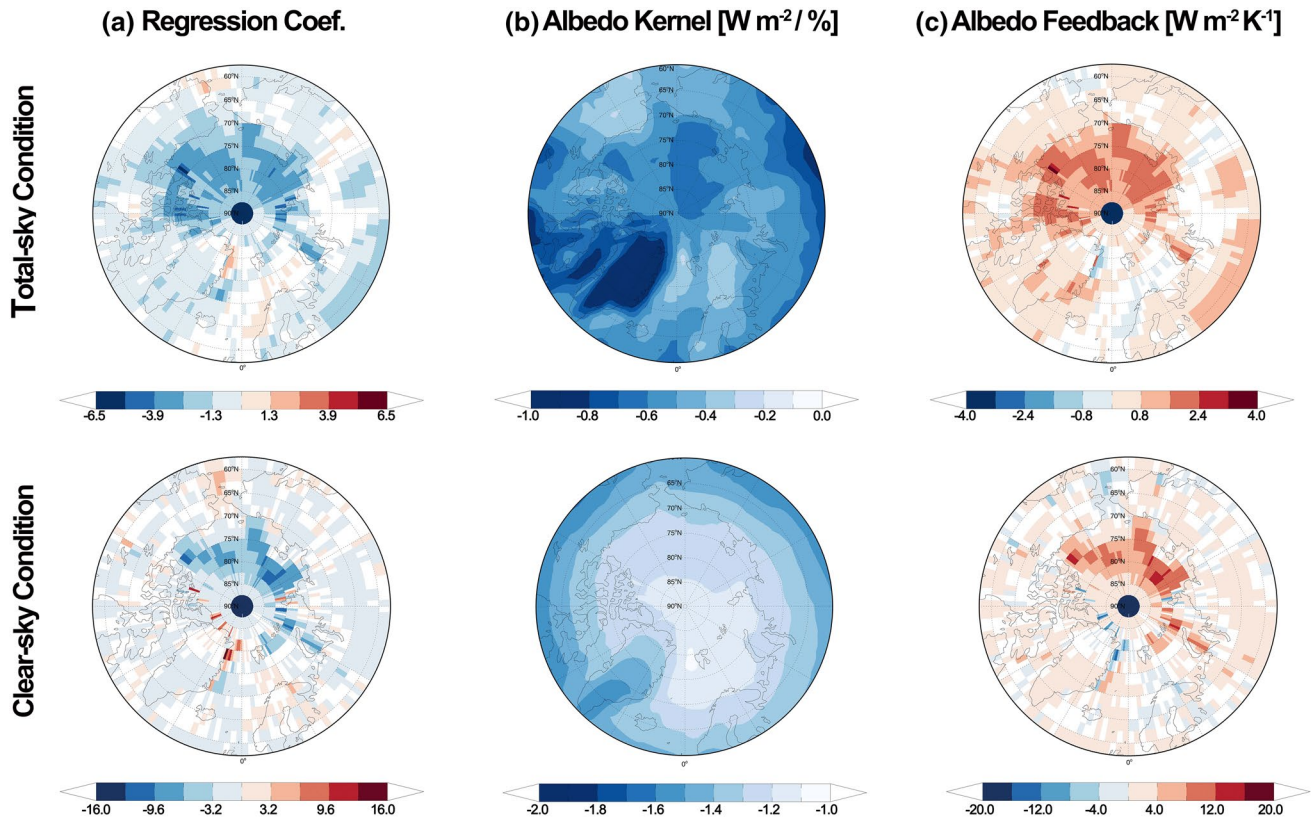


**Fig. 4** Distribution map of **a** regression slope of  $\Delta\tilde{\alpha}$  versus  $\Delta\tilde{T}_s$ , **b** annual mean albedo kernel ( $\text{W m}^{-2}\%$ ), and **c** albedo feedback

( $\text{W m}^{-2} \text{K}^{-1}$ ) at the total-sky (top) and clear-sky condition (bottom) over the Northern high-latitude regions. White areas indicate insignificant values at the 95% level, as determined by Student's *t* test

less SW radiation being absorbed by the system (Fig. 4b). Following Eq. (4), the albedo feedback parameter at each grid point in Fig. 4c is calculated as the product of the regression slope in Fig. 4a, and the surface albedo kernel in Fig. 4b. In the all sky condition, the surface albedo kernel strongly depends on geographic location; whereas in the clear-sky condition, it is approximately a function of latitude. We found that the positive albedo feedback is concentrated mainly on the Arctic Ocean area, especially the Chukchi and Beaufort Seas (Fig. 4c).

To understand the contribution of vertical temperature profiles to local radiative feedback, Fig. 5 shows the zonally averaged vertical profiles of the differential temperature response to the increased SAT, temperature kernel, and lapse rate feedback. Figure 5a shows the zonally averaged regression slope of  $\Delta(\tilde{T} - \tilde{T}_s)/\Delta\tilde{T}_s$ . As the altitude increases, the temperature difference increases, especially at the latitudes northward of 70°N. This suggests that the temperature is strongly stratified at the higher latitude and upper troposphere. The temperature kernel is annually and zonally averaged, which describes the response of TOA LW radiation being absorbed by the

system to increase in surface temperatures (Fig. 5b). Relatively stronger negative values are distributed in the upper troposphere around 60°N, and the lower troposphere around 90°N. The lapse rate feedback is related to the changes in temperature difference between the upper level and the surface. According to Eq. (6), the product of the regression slope (Fig. 5a) and the radiative kernel (Fig. 5b) results in the positive lapse rate feedback (Fig. 5c). These results imply that the considerable warming at the surface remains confined to the lower parts of the atmosphere.

Figure 6 shows the latitude-height distribution of the water vapor profiles. A positive water vapor kernel indicates that the increase in water vapor derives increases in TOA LW radiation being absorbed by the system (Fig. 6b). The water vapor kernel is comparatively small in high latitude regions due to the small amount of water vapor, and it possibly becomes negative at the lower part of the atmosphere, because strong surface inversion acts to decrease the net LW fluxes (Yamanouchi and Kawaguchi 1984; Soden et al. 2008). Figure 6a shows that most water vapor changes occur in the lower part of the

altitude increases, the temperature difference increases, especially at the latitudes northward of 70°N. This suggests that the temperature is strongly stratified at the higher latitude and upper troposphere. The temperature kernel is annually and zonally averaged, which describes the response of TOA LW radiation being absorbed by the

**Fig. 5** Zonal mean **a** regression slope of  $\Delta(\tilde{T} - \tilde{T}_s)$  with  $\Delta\tilde{T}_s$ , **b** annual mean temperature kernel ( $\text{W m}^{-2} \text{K}^{-1}/100 \text{ hPa}$ ), and **c** lapse rate feedback ( $\text{W m}^{-2} \text{K}^{-1}/100 \text{ hPa}$ ) over the Northern high-latitude regions. White areas indicate insignificant values at the 95% level, as determined by Student's *t* test

atmosphere, and over the Arctic regions, where low-level liquid-containing clouds are frequently observed (Cesana et al. 2012). This implies that increasing water vapor acts to increase cloud formation, which leads to negative feedback at the lower part of the atmosphere. Consequently, water vapor exerts overall weak positive feedback at high-latitude, but it can also partially serve as a weak negative feedback at latitudes greater than 70°N (Fig. 6c).

Figure 7 summarizes the estimated individual local radiative feedback parameters. In the absence of clouds (clear sky), the SW radiation is predominantly controlled by the surface albedo feedback by  $+1.13 \pm 0.44 \text{ W m}^{-2} \text{ K}^{-1}$ . However, in the presence of clouds (all sky), the surface albedo feedback parameter is  $+0.49 \pm 0.30 \text{ W m}^{-2} \text{ K}^{-1}$ , i.e., a 43% decrease from clear-sky to all-sky cases. Based on Eq. (7a), cloud feedback is associated with difference between surface albedo feedback for the clear-sky and all-sky conditions. Consequently, clouds represent negative radiative feedback of  $-0.41 \pm 1.00 \text{ W m}^{-2} \text{ K}^{-1}$  (Fig. 7a). This is because clouds cancel out the positive surface albedo feedback by interfering with the influence of any underlying change in the surface albedo (Kato et al. 2006; Soden et al. 2008).

In the LW radiative feedback process, a water vapor feedback is approximated to the product of water vapor kernel and response of the water vapor to the changing surface temperature based on Eq. (5). The water vapor feedback value of  $+0.08 \pm 0.02 \text{ W m}^{-2} \text{ K}^{-1}$  is small enough to be neglected, as it has little effect on the radiative response of TOA LW radiation to changes in water vapor at the low troposphere, despite the considerable changes in water vapor in the lowermost atmosphere. Also, the clouds slightly reduce the water vapor feedback by about  $0.14 \text{ W m}^{-2} \text{ K}^{-1}$ , while they slightly increase the lapse rate feedback by about  $0.41 \text{ W m}^{-2} \text{ K}^{-1}$ ; accordingly, the cloud feedback ( $0.19 \pm 0.52 \text{ W m}^{-2} \text{ K}^{-1}$ ) acts as a trivial positive feedback in the LW feedback process. Consequently, the lapse rate feedback ( $1.33 \pm 0.18 \text{ W m}^{-2} \text{ K}^{-1}$ ) plays a major role in regulating LW radiation, which confirms previous studies (Graversen et al. 2014; Pithan and Mauritsen 2014) (Fig. 7b).

The changes in temperature difference between the upper level and surface are the underlying cause of the lapse rate feedback process. In general, the global lapse rate feedback is known to be negative, which stabilizes the climate. On the other hand, our result shows that the

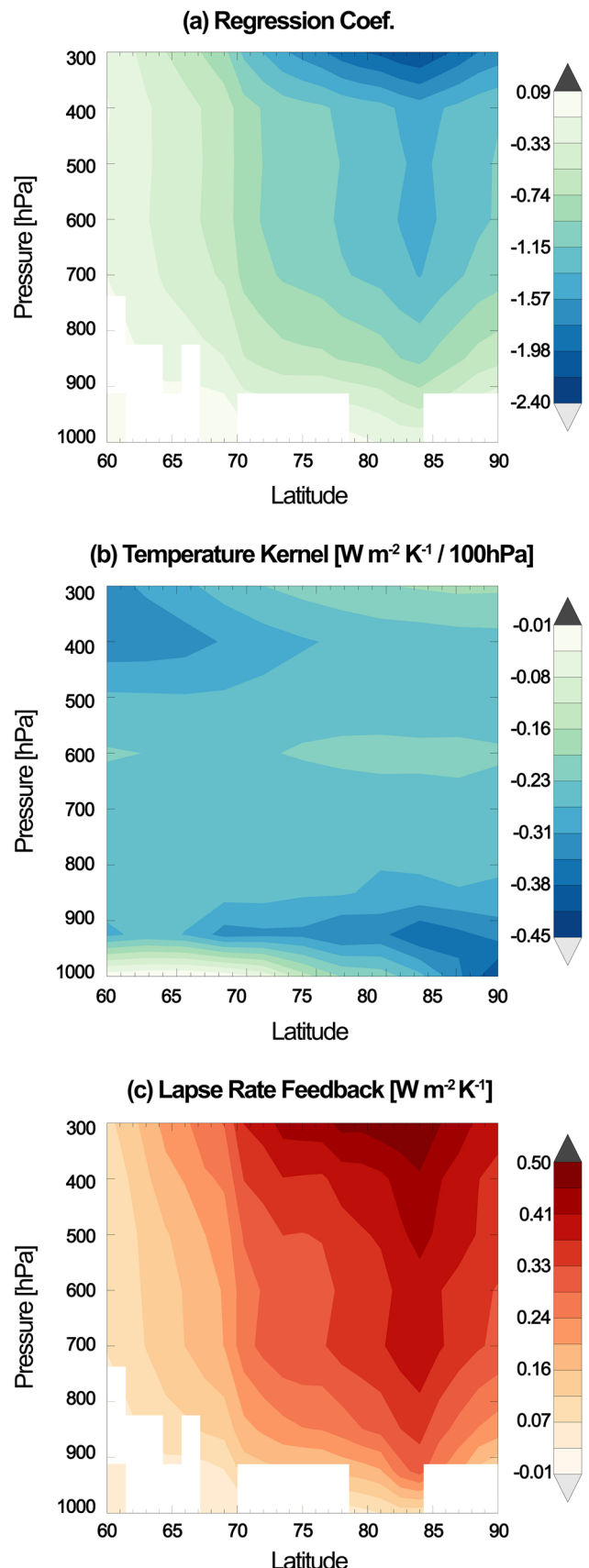


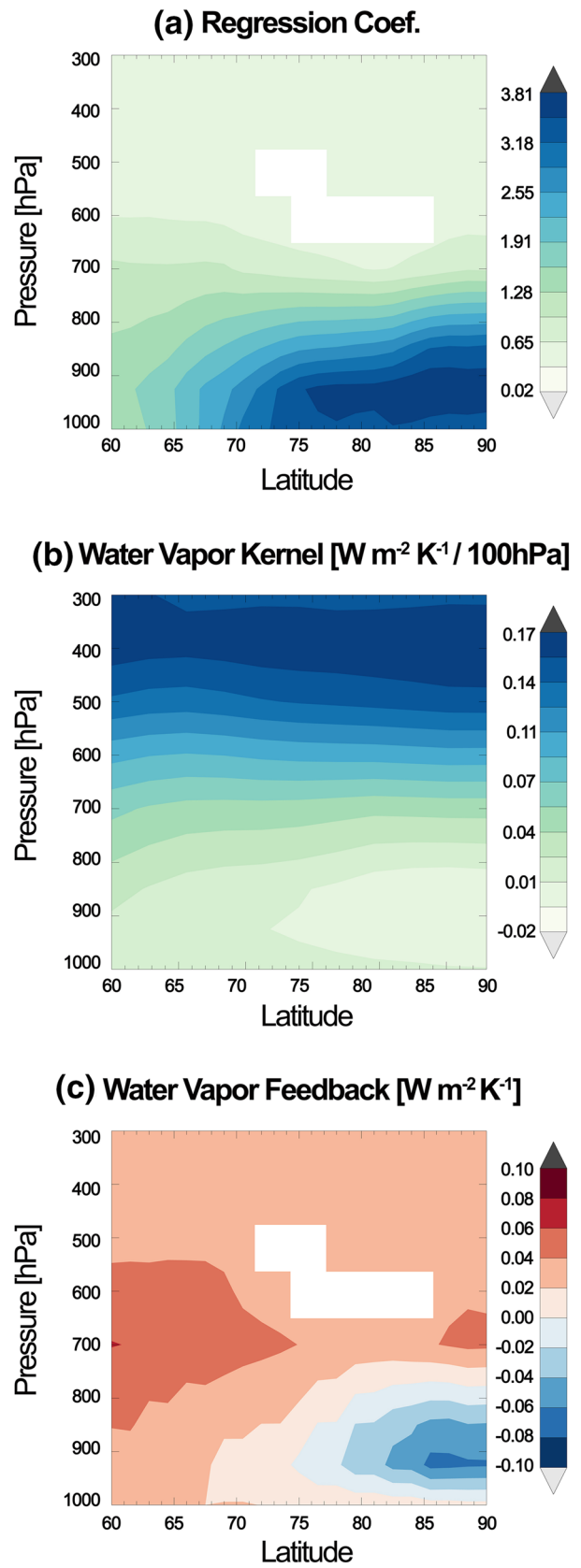
**Fig. 6** Zonal mean **a** regression slope of  $\Delta\tilde{q}$  with  $\Delta\tilde{T}_s$ , **b** annual mean water vapor kernel ( $\text{W m}^{-2} \text{K}^{-1}/100 \text{hPa}$ ), and **c** water vapor feedback ( $\text{W m}^{-2} \text{K}^{-1}/100 \text{hPa}$ ) over the Northern high-latitude regions. White areas indicate insignificant values at the 95% level, as determined by Student's *t* test

lapse rate in NHL acts as a strong positive feedback effect (also refer to Manabe and Wetherald 1975). Figures 5a and 6a show that as the altitude increases, the amount of water vapor reduces and the temperature drops, especially within the  $75^\circ\text{N}$ – $90^\circ\text{N}$  regions, where extremely cold temperatures are found in the lower parts of the atmosphere. The cold and heavy air near the surface is hardly coupled with the upper atmosphere; moreover, the dry background atmosphere produces relatively less atmospheric emission. The enhanced atmospheric stratification at latitude greater than  $70^\circ\text{N}$  produces bottom-heavy warming profiles, and the lapse rate feedback strongly reinforces NHL warming. However, the quantitative estimation of the interaction needs further attention, as the lapse rate feedback and surface albedo feedback can actively interact with each other (Graversen et al. 2014).

The residuals represent large values in both the SW and LW radiative feedback processes (Fig. 7). Non-local or non-radiative feedback processes, i.e., the nonlinearity among the individual feedback processes, atmospheric heat transports from the mid or low latitude, and seasonal variations in heat energy from the Arctic oceans, can be contained in the residual values (Kim et al. 2015). However, a positive radiative feedback parameter tends to be overestimated, if the local domain has a lower surface heat capacity compared to the ocean-covered region, or the dynamical heat transport actively contributes to the TOA radiative perturbations. Moreover, it appears that some portion of the residual originates from the underestimation of the SW radiative feedbacks in the reanalysis data, which will be further discussed.

#### 4 Conclusions and discussion

In this study, variations in satellite-observed radiations and the surface air temperature were used to estimate the local radiative feedback parameters over the NHL regions. The NHL region contains significant non-feedback factors, such as strong seasonality and autonomous cloud variation, with feedback processes of time spanning longer than a month. In order to overcome these limits and to estimate the local radiative feedback parameters with accuracy, we adopted the 12-month moving average over the time-series that is deseasonalized against monthly climatology, and area-averaged over the NHL ( $\langle\widetilde{R}_{SW}^\dagger\rangle$ ,  $\langle\widetilde{R}_{LW}^\dagger\rangle$ , and  $\langle\widetilde{T}_s\rangle$ ). Then,



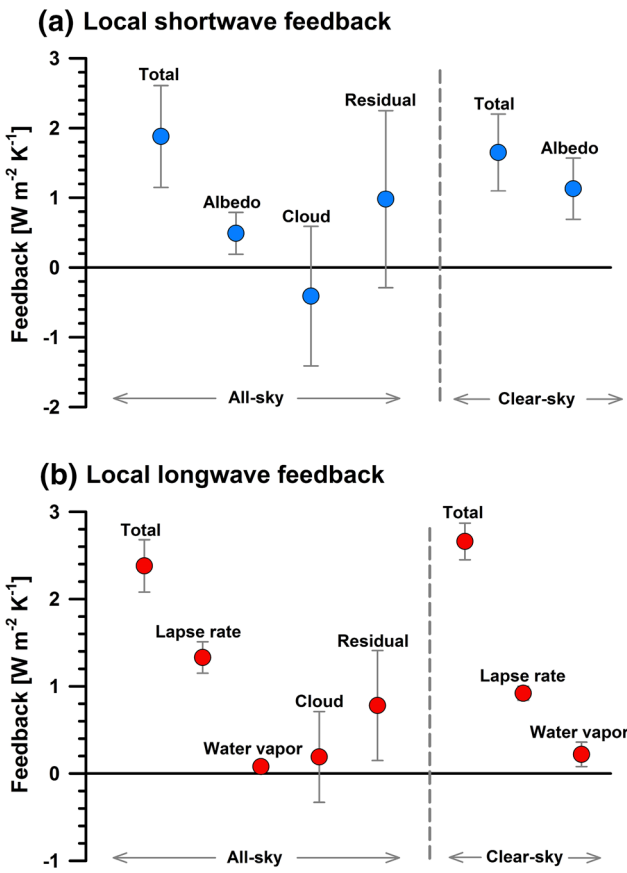


**Fig. 7** Decomposition of **a** total shortwave, and **b** longwave radiative feedback into individual feedback components by the radiative kernel. Each of the individual feedback components originates from the change in surface albedo, water vapor, lapse rate, and clouds, in units of  $\text{W m}^{-2} \text{K}^{-1}$

the simple lagged linear regression slopes on the  $\langle \widetilde{R}_{SW}^{\uparrow} \rangle$  and  $\langle \widetilde{R}_{LW}^{\uparrow} \rangle$ , with the  $\langle \widetilde{T}_s \rangle$  indicate the local SW and LW radiative feedback parameters, respectively. Consequently, the estimated values of the local radiative feedback parameters are  $+1.88 \pm 0.73 \text{ W m}^{-2} \text{ K}^{-1}$  for SW radiation, and  $+2.38 \pm 0.30 \text{ W m}^{-2} \text{ K}^{-1}$  for LW radiation. One might question whether the uncertainties of the observational data could impact confidence in the results. For example, CERES errors, which are stated to be 5% for shortwave and 1% for longwave, seem to be in the same order of changes in radiation (i.e. 10 and  $2 \text{ W m}^{-2}$ , respectively). However, our estimates are based on the relative perturbation of radiative fluxes; therefore, the values of systematic error cannot be directly compared with our estimates.

By representing the quantitative estimation of the feedback values based on observation, we demonstrated that the cloud and lapse rate feedbacks serve as a major contributor to the total radiative feedback over NHL. Much of the total radiative feedback is not explained by the simple sum

of the individual SW and LW radiative feedbacks, implying the important role of nonlinear interaction between the different processes. The surface albedo feedback, which is known to be the main element of SW radiation, plays a considerable role under the cloud-free condition; however, under the cloud sky condition, surface albedo feedback diminishes, due to cloud and surface albedo interaction. This leads to negatively enhanced total cloud feedback ( $0.22 \pm 1.52 \text{ W m}^{-2} \text{ K}^{-1}$ ). A remarkable aspect of the LW radiative feedback is that the lapse rate feedback strongly affects the high latitude amplification. This is because the extreme dryness of the atmosphere and strong surface warming enhances atmospheric stratification, by producing a bottom-heavy warming profile. Although some studies have pointed out that surface warming by the meridional atmospheric energy transport and heat transport from the Arctic oceans occupies a significant portion of the LW feedback process (Alexeev et al. 2005; Langen and Alexeev 2007; Spielhagen et al. 2011), it is not explicitly estimated, but is contained as part of the residuals.

The major factors that lead to the large residual values are suggested to be as follows. Firstly, the underestimated variability of climate variables from the reanalysis data could contribute to the residuals. The perturbations of TOA radiations from ERA-Interim reanalysis do not correspond to those from the CERES satellite measurements (Masters 2012), especially within the NHL, where the discrepancy in SW radiation is large. The total radiative feedback estimation based on the TOA radiations from ERA-Interim reanalysis data tends to underestimate the total SW radiative feedback by  $1.24 \pm 1.29 \text{ W m}^{-2} \text{ K}^{-1}$  and the LW radiative feedback by  $0.3 \pm 0.66 \text{ W m}^{-2} \text{ K}^{-1}$ , compared to the results of this study, which are estimated from satellite observed radiations. Thus in the reanalysis, the climate variables that modulate the TOA radiative perturbations could be less variable than they are in reality. Since the individual feedbacks are estimated from the variability of climate variables, there is a possibility that the individual feedbacks could be underestimated. Consequently, this can result in large residuals (underestimated SW radiative feedback values exceed the SW residuals, and underestimated LW feedback values have an approximately 37.5% share of LW residuals). Secondly, the unresolved nonlinearity among the individual feedback processes can be included in residual terms. Although the individual feedback components are linearly separated using a radiative kernel, the changes in surface air temperature are nonlinearly inter-related with various climate variables (Kay and Gettelman 2009; Graversen et al. 2014). Hence, the sum of individual feedbacks can somewhat differ from the total radiative feedback value. Furthermore, the local radiative variability to surface air temperature is affected by nonlinear dynamic feedback processes, such as changes in clouds, atmospheric heat

convergence, and seasonal variations in heat energy from the Arctic oceans. Accordingly, the nonlinear dynamic feedback processes also contribute to the residual values (Kim et al. 2015; Brown et al. 2016). Thus, a quantitative separation of the residuals into the contribution of nonlinearity, and the influence of heat transport in the atmosphere and the Arctic oceans, would be a subject of future study.

The uncertainties of the feedback values mainly arise from the local heat transport and randomly varying clouds, which blur the simultaneous covariance between radiation and temperature. Also, the inaccuracy of the cloud fraction in the radiative kernel could contribute to the uncertainties of cloud feedbacks, as well as the residuals. Since as suggested by Soden et al. (2008), the cloud feedback was indirectly calculated from the difference between the all-sky and clear-sky kernels, the estimated values of cloud feedback strongly depend on the experimental condition of the cloud fraction in the climate model. Although Zelinka et al. (2012) developed a technique for quantifying cloud feedback based on simulated cloud radiative kernel, this study did not focus on the calculation of the feedback value itself, but on the relative comparisons among the individual feedbacks. Still, it is especially noteworthy that the cloud effect associated with surface albedo feedback in the current climate models differs from that of the satellite-based observation; therefore, the physical relationship between clouds and surface albedo should be further investigated (Choi et al. 2014c).

Nevertheless, the estimated magnitude of the total and individual local radiative feedback using satellite-based observations in this study will serve as an effective indicator to evaluate the degree of accuracy of the simulation of the local radiative feedback process over NHL by the existing climate models.

**Acknowledgements** This research was supported by the GEMS program of the Ministry of Environment, Korea and the Eco Innovation Program of KEITI (2012000160003) and the Korea Meteorological Administration Research and Development Program, under Grant KMIPA2015-6110. Authors Y.-S. Choi, J. H. Jiang, and H. Su acknowledge the support of the Jet Propulsion Laboratory, California Institute of Technology, sponsored by the National Aeronautics and Space Administration (NASA). W. Kim acknowledges the support of the APEC Climate Center. The authors thank the Clouds and the Earth's Radiant Energy System (CERES) and ERA-Interim reanalysis data production teams for providing their data.

## References

- Alexeev V, Langen PL, Bates JR (2005) Polar amplification of surface warming on an aquaplanet in “ghost forcing” experiments without sea ice feedbacks. *Clim Dyn* 24:655–666
- Brown PT, Li W, Jiang JH, Su H (2016) Unforced surface air temperature variability and its contrasting relationship with the anomalous TOA energy flux at local and global spatial scales. *J Clim* 29:925–940
- Burt MA, Randall DA, Branson MD (2016) Dark warming. *J Clim* 29:705–719
- Cesana G, Kay J, Chepfer H, English J, Boer G (2012) Ubiquitous low-level liquid-containing Arctic clouds: new observations and climate model constraints from CALIPSO-GOCCP. *Geophys Res Lett* 39
- Cess RD (1976) Climate change: an appraisal of atmospheric feedback mechanisms employing zonal climatology. *J Atmos Sci* 33:1831–1843
- Chapin FS, Randerson JT, McGuire AD, Foley JA, Field CB (2008) Changing feedbacks in the climate–biosphere system. *Front Ecol Environ* 6:313–320
- Choi Y-S, Song H-J (2012) On the numerical integration of a randomly forced system: variation and feedback estimation. *Theor Appl Climatol* 110:97–101
- Choi Y-S, Ho C-H, Park C-E, Storelvmo T, Tan I (2014a) Influence of cloud phase composition on climate feedbacks. *J Geophys Res* 119:3687–3700
- Choi Y-S, Kim B-M, Hur S-K, Kim S-J, Kim J-H, Ho C-H (2014b) Connecting early summer cloud-controlled sunlight and late summer sea ice in the Arctic. *J Geophys Res* 119
- Choi Y-S, Cho H, Ho C-H, Lindzen RS, Park SK, Yu X (2014c) Influence of non-feedback variations of radiation on the determination of climate feedback. *Theor Appl Climatol* 115:355–364
- Christensen MW, Behrangi A, L'Ecuyer T, Wood NB, Lebsack MD, Stephens GL (2016) Arctic observation and reanalysis integrated system: a new data product for validation and climate study. *Bull Am Meteorol Soc*
- Chylek P, Folland CK, Lesins G, Dubey MK, Wang M (2009) Arctic air temperature change amplification and the Atlantic Multidecadal Oscillation. *Geophys Res Lett* 36
- Comiso JC, Hall DK (2014) Climate trends in the Arctic as observed from space. *WIREs Clim Change* 5:389–409
- Cronin TW, Tziperman E (2015) Low clouds suppress Arctic air formation and amplify high-latitude continental winter warming. *Proc Natl Acad Sci USA* 112:11490–11495
- Dee D, Uppala S, Simmons A, Berrisford P, Poli P, Kobayashi S, Andrae U, Balmaseda M, Balsamo G, Bauer P (2011) The ERA-Interim reanalysis: Configuration and performance of the data assimilation system. *Q J R Meteorol Soc* 137:553–597
- Dessler A (2013) Observations of climate feedbacks over 2000–10 and comparisons to climate models. *J Clim* 26:333–342
- Donohoe A, Armour KC, Pendergrass AG, Battisti DS (2014) Shortwave and longwave radiative contributions to global warming under increasing CO<sub>2</sub>. *Proc Natl Acad Sci USA* 111:16700–16705
- Eastman R, Warren SG (2010) Arctic cloud changes from surface and satellite observations. *J Clim* 23:4233–4242
- Forster PMF, Gregory JM (2006) The climate sensitivity and its components diagnosed from Earth radiation budget data. *J Clim* 19:39–52
- Frankignoul C (1999) A cautionary note on the use of statistical atmospheric models in the middle latitudes: comments on “Decadal variability in the North Pacific as simulated by a hybrid coupled model”. *J Clim* 12:1871–1872
- Frankignoul C, Czaja A, L'Heverder B (1998) Air-sea feedback in the North Atlantic and surface boundary conditions for ocean models. *J Clim* 11:2310–2324
- Ghatak D, Miller J (2013) Implications for Arctic amplification of changes in the strength of the water vapor feedback. *J Geophys Res* 118:7569–7578

- Graversen RG, Mauritsen T, Tjernström M, Källén E, Svensson G (2008) Vertical structure of recent Arctic warming. *Nature* 451:53–56
- Graversen RG, Langen PL, Mauritsen T (2014) Polar amplification in CCSM4: Contributions from the lapse rate and surface albedo feedbacks. *J Clim* 27:4433–4450
- Gregory J, Ingram W, Palmer M, Jones G, Stott P, Thorpe R, Lowe J, Johns T, Williams K (2004) A new method for diagnosing radiative forcing and climate sensitivity. *Geophys Res Lett* 31
- Hall A (2004) The role of surface albedo feedback in climate. *J Clim* 17:1550–1568
- Hansen J, Lacis A, Rind D, Russell G, Stone P, Fung I, Ruedy R, Lerner J (1984) Climate sensitivity: analysis of feedback mechanisms. In: Hansen JE, Takahashi T (eds) *Climate processes and climate sensitivity*. American Geophysical Union, Washington DC, pp 130–163
- Hansen J, Nazarenko L, Ruedy R, Sato M, Willis J, Del Genio A, Koch D, Lacis A, Lo K, Menon S (2005) Earth's energy imbalance: confirmation and implications. *Science* 308:1431–1435
- Holland MM, Bitz CM (2003) Polar amplification of climate change in coupled models. *Clim Dyn* 21:221–232
- Hwang YT, Frierson DM, Kay JE (2011) Coupling between Arctic feedbacks and changes in poleward energy transport. *Geophys Res Lett* 38
- Jonko AK, Shell KM, Sanderson BM, Danabasoglu G (2012) Climate feedbacks in CCSM3 under changing CO<sub>2</sub> forcing. Part I: adapting the linear radiative kernel technique to feedback calculations for a broad range of forcings. *J Clim* 25:5260–5272
- Kato S, Loeb NG, Minnis P, Francis JA, Charlock TP, Rutan DA, Clothiaux EE, Sun-Mack S (2006) Seasonal and interannual variations of top-of-atmosphere irradiance and cloud cover over polar regions derived from the CERES data set. *Geophys Res Lett* 33
- Kay JE, Gettelman A (2009) Cloud influence on and response to seasonal Arctic sea ice loss. *J Geophys Res.* doi:[10.1029/2009JD011773](https://doi.org/10.1029/2009JD011773)
- Kay JE, L'Ecuyer T (2013) Observational constraints on Arctic Ocean clouds and radiative fluxes during the early 21st century. *J Geophys Res* 118:7219–7236
- Kim Y, Choi Y-S, Kim B-M, Kim H (2015) Influence of altered low cloud parameterizations for seasonal variation of Arctic cloud amount on climate feedbacks. *Clim Dyn* 47:1661–1672
- Knutti R, Hegerl GC (2008) The equilibrium sensitivity of the Earth's temperature to radiation changes. *Nat Geosci* 1:735–743
- Langen PL, Alexeev VA (2007) Polar amplification as a preferred response in an idealized aquaplanet GCM. *Clim Dyn* 29:305–317
- Lindzen RS, Choi Y-S (2009) On the determination of climate feedbacks from ERBE data. *Geophys Res Lett* 36
- Lindzen RS, Choi Y-S (2011) On the observational determination of climate sensitivity and its implications. *Asia Pac J Atmos Sci* 47:377–390
- Manabe S, Wetherald RT (1975) The effect of doubling the CO<sub>2</sub> concentration on the climate of a general circulation model
- Masters T (2012) On the determination of the global cloud feedback from satellite measurements. *Earth Syst Dyn* 3:97–107
- Meehl GA, Teng H, Arblaster JM (2014) Climate model simulations of the observed early-2000s hiatus of global warming. *Nat Clim Change* 4:898–902
- Murphy DM (2010) Constraining climate sensitivity with linear fits to outgoing radiation. *Geophys Res Lett* 37
- Pithan F, Mauritsen T (2014) Arctic amplification dominated by temperature feedbacks in contemporary climate models. *Nat Geosci* 7:181–184
- Rigor IG, Colony RL, Martin S (2000) Variations in surface air temperature observations in the Arctic, 1979–97. *J Clim* 13:896–914
- Rind D (2008) The consequences of not knowing low-and high-latitude climate sensitivity. *Bull Am Meteorol Soc* 89:855
- Santer BD, Bonfils C, Painter JF, Zelinka MD, Mears C, Solomon S, Schmidt GA, Fyfe JC, Cole JN, Nazarenko L (2014) Volcanic contribution to decadal changes in tropospheric temperature. *Nat Geosci* 7:185–189
- Screen JA, Simmonds I (2010) The central role of diminishing sea ice in recent Arctic temperature amplification. *Nature* 464:1334–1337
- Sedlar J, Tjernström M, Mauritsen T, Shupe MD, Brooks IM, Persson POG, Birch CE, Leck C, Sirevaag A, Nicolaus M (2011) A transitioning Arctic surface energy budget: the impacts of solar zenith angle, surface albedo and cloud radiative forcing. *Clim Dyn* 37:1643–1660
- Serreze M, Barrett A, Stroeve J, Kindig D, Holland M (2009) The emergence of surface-based Arctic amplification. *Cryosphere* 3:11
- Shell KM, Kiehl JT, Shields CA (2008) Using the radiative kernel technique to calculate climate feedbacks in NCAR's Community Atmospheric Model. *J Clim* 21:2269–2282
- Skific N, Francis JA (2013) Drivers of projected change in Arctic moist static energy transport. *J Geophys Res* 118:2748–2761
- Soden BJ, Held IM (2006) An assessment of climate feedbacks in coupled ocean-atmosphere models. *J Clim* 19:3354–3360
- Soden BJ, Held IM, Colman R, Shell KM, Kiehl JT, Shields CA (2008) Quantifying climate feedbacks using radiative kernels. *J Clim* 21:3504–3520
- Spencer RW, Braswell WD (2011) On the misdiagnosis of surface temperature feedbacks from variations in Earth's radiant energy balance. *Remote Sens* 3:1603–1613
- Spielhagen RF, Werner K, Sørensen SA, Zamelczyk K, Kandiano E, Budeus G, Husum K, Marchitto TM, Hald M (2011) Enhanced modern heat transfer to the Arctic by warm Atlantic water. *Science* 331:450–453
- Trenberth KE, Zhang Y, Fasullo JT, Taguchi S (2015) Climate variability and relationships between top-of-atmosphere radiation and temperatures on Earth. *J Geophys Res* 120:3642–3659
- van der Linden E, Bintanja R, Hazeleger W, Katsman C (2014) The role of the mean state of Arctic Sea ice on near-surface temperature trends. *J Clim* 27:2819–2841
- Vavrus S (2004) The impact of cloud feedbacks on Arctic climate under greenhouse forcing. *J Clim* 17:603–615
- Wielicki BA, Barkstrom BR, Harrison EF, Lee III RB, Louis Smith G, Cooper JE (1996) Clouds and the Earth's Radiant Energy System (CERES): an earth observing system experiment. *Bull Am Meteorol Soc* 77:853–868
- Winton M (2008) Sea ice—albedo feedback and nonlinear Arctic climate change. *Arctic Sea Ice Decline*. American Geophysical Union, Washington, DC, pp 111–131
- Yamanouchi T, Kawaguchi S (1984) Longwave radiation balance under a strong surface inversion in the Katabatic Wind Zone, Antarctica. *J Geophys Res* 89:11771–11778
- Zelinka MD, Klein SA, Hartmann DL (2012) Computing and partitioning cloud feedbacks using cloud property histograms. Part I: cloud radiative kernels. *J Clim* 25:3715–3735